AGU PUBLICATIONS

JGR

Journal of Geophysical Research: Earth Surface

RESEARCH ARTICLE

10.1002/2013JF002833

Key Points:
- We analyze sediment transport in a CA model using a particle tracking technique
- Barchan dunes are not well-mixed reservoirs
- The central longitudinal dune slice controls the barchan morphodynamics

Correspondence to:
C. Narteau,
narteau@ipgp.fr

Citation:
Zhang, D., X. Yang, O. Rozier, and C. Narteau (2014), Mean sediment residence time in barchan dunes, *J. Geophys. Res. Earth Surf.*, *119*, 451–463, doi:10.1002/2013JF002833.

Received 24 APR 2013
Accepted 19 JAN 2014
Accepted article online 28 JAN 2014
Published online 11 MAR 2014

Mean sediment residence time in barchan dunes

D. Zhang[1], X. Yang[1], O. Rozier[2], and C. Narteau[2]

[1]Chinese Academy of Sciences Key Laboratory of Cenozoic Geology and Environment, Institute of Geology and Geophysics, CAS, Beijing, China, [2]Institut de Physique du Globe de Paris UMR 7154, CNRS, Université Paris 7, Paris, France

Abstract When a barchan dune migrates, the sediment trapped on its lee side is later mobilized when exposed on the stoss side. Then sand grains may undergo many dune turnover cycles before their ejection along the horns, but the amount of time a sand grain contributes to the dune morphodynamics remains unknown. To estimate such a residence time, we analyze sediment particle motions in steady state barchans by tracking individual cells of a 3-D cellular automaton dune model. The overall sediment flux may be decomposed into advective and dispersive fluxes to estimate the relative contribution of the underlying physical processes to the barchan shape. The net lateral sediment transport from the center to the horns indicates that dispersion on the stoss slope is more efficient than the convergent sediment fluxes associated with avalanches on the lee slope. The combined effect of these two antagonistic dispersive processes restricts the lateral mixing of sediment particles in the central region of barchans. Then, for different flow strengths and dune sizes, we find that the mean residence time of sediment particles in barchans is equal to the surface of the central longitudinal dune slices divided by the input sand flux. We infer that this central slice contains most of the relevant information about barchan morphodynamics. Finally, we initiate a discussion about sediment transport and memory in the presence of bed forms using the advantages of the particle tracking technique.

1. Introduction

A large number of disciplines in natural sciences aim to understand how and how long it takes sediments to move through geomorphic systems. Indeed, as tectonics, erosion, and deposition shape the surface of the Earth, the storage times and the motions of individual particles are precious sources of information about the characteristic time scales of a wide range of physical and chemical processes. On geological timescales, this knowledge relies almost entirely on dating methods using radioactive isotopes (e.g., uranium-thorium for exhumation rate [*Dosseto et al.*, 2008; *Vigier et al.*, 2001]), cosmogenic nuclides (e.g., ^{10}Be for erosion rate in drainage networks [*Brown et al.*, 1995; *Gayer et al.*, 2008]), and more recently, luminescence (e.g., optically stimulated luminescence for residence time in dunes [*Lancaster*, 2008; *Yang et al.*, 2012]). If these methods have different degrees of uncertainty inherent to measurements, they are also difficult to perform on a large number of samples because of their human and financial costs. Hence, it is often difficult to assess the robustness of the age estimates with respect to the underlying assumptions and the reproducibility of the results. On shorter time scales, various types of particle-tracking techniques have been used successfully to analyze sediment dispersion in natural systems (e.g., image processing, solute, and particle tracers such as radio-tagged rocks [*Schmidt and Ergenzinger*, 1992]). Especially developed for transport-related issues [*Van Rijn*, 1993], these techniques yield reasonable estimates of the probability distribution function of the distance traveled by a grain. Unfortunately, they can rarely be used to investigate the mode of entrainment, the burial depth history, and the temporal distribution of the successive episodes of transport. In this case, along with the improvement of computer technology, numerical models have become a complementary approach to investigate sediment dispersion and particle motions through geomorphic systems.

Despite a growing number of observations and the development of modeling methods, sediment transport and residence time in the presence of bed forms are still open issues [*Vermeesch et al.*, 2010]. For example, even if the overall bedload transport may be approximated from the dune velocity [*Bagnold*, 1941], a fundamental difficulty remains to estimate how these bed forms affect the motion and the storage of sedimentary particles. There is still no satisfactory residence time distribution or transport law to describe the migration of individual grains in sedimentary layers sheared by a fluid flow. In this paper, we start to address these questions using a discrete computational method and an isolated barchan, the most studied object in the physics of sand dunes [*Howard et al.*, 1978; *Hersen et al.*, 2002; *Andreotti et al.*, 2002; *Momiji et al.*, 2002; *Sauermann et al.*, 2003; *Hersen*, 2004a, 2005].

Barchans form in sediment supply-limited regions submitted to unidirectional flows [*Wasson and Hyde*, 1983; *Pye and Tsoar*, 1990]. They are isolated crescentic structures with horns extending downwind on both sides of a sand pile characterized by a slip face in the lee. Above a threshold wind velocity at which sand grains start to move, bed load transport occurs on the windward face, which usually exhibits a slope of approximately 10°. The slip face is the result of avalanches of grains from the dune crest. The angle of repose of sand being approximately of 34°, the dune profile is asymmetric in the direction of the wind and a region of flow separation forms in the lee of the dune. The slip face is not exposed to the primary flow and acts as a sediment trap. There are also strong lateral variations in the barchan shape. The crest is perpendicular to the wind in the center and tends to be parallel to the flow along horns as the longitudinal dune height is decreasing. Ultimately, the slip face disappears at the horn terminations where the longitudinal profile of barchans has a dome shape with smooth, gently curving topography. For such a low and elongated topographic profile, the absence of recirculation zones results in the emission of sand grains at a rate which is close to the saturated flux Q_{sat} measured upstream on a flat sand bed. Hence, a barchan needs to be fed by an input sediment flux to propagate downstream with constant shape and speed.

Barchans have been observed in many geophysical environments on Earth (arid deserts, icecaps, and under water) and Mars, as well as in various types of laboratory experiments [*Finkel*, 1959; *Hastenrath*, 1987; *Edgett and Blumberg*, 1994; *Hesp and Hastings*, 1998; *Hersen et al.*, 2002; *Groh et al.*, 2008; *Bourke*, 2010; *Birnbaum et al.*, 2010; *Franklin and Charru*, 2011; *Taniguchi et al.*, 2012; *Bridges et al.*, 2012]. In all cases, the same relationships can be found between their characteristic dimensions and propagation speed, suggesting that whatever the physical environments, they are driven by similar underlying mechanisms [*Claudin and Andreotti*, 2006]. For example, assuming that all the sediment that passes the crest is captured in a well-established recirculation zone, the equation of conservation of mass can be used to estimate the migration speed c of barchans with respect to their height H_∞

$$c \propto \frac{Q_{crest}}{H_\infty} \tag{1}$$

where Q_{crest} is the sand flux at the crest which is known to be proportional to Q_{sat} [*Elbelrhiti et al.*, 2005; *Gao et al.*, 2013]. Thus, smaller barchans are faster than bigger ones and, within dune fields, collisions are frequent and may result in the formation of larger structures or secondary bed forms. An important time scale of an isolated barchan is also the amount of time it takes for all the sediment to be remobilized. Assuming that the barchan shape is scale-invariant, such a renewal time can be expressed as

$$T_d \propto \frac{L_\infty}{c} \tag{2}$$

where L_∞ is the length of the dune.

The last decades have been a flourishing period for understanding the physics of sand dunes and the development of continuous and discrete numerical dune models [*Nishimori and Ouchi*, 1993; *Werner and Gillespie*, 1993; *Werner*, 1995; *Nishimori et al.*, 1998; *Momiji and Warren*, 2000; *Sauermann et al.*, 2001; *Kroy et al.*, 2002; *Fischer et al.*, 2008; *Parteli et al.*, 2011]. Based on a set of differential equations, continuous models allow a systematical investigation of the dynamic equilibrium between the topography, the flow, and the motion of sediment particles. Nevertheless, there are several open issues, mainly related to modeling flow separation at brinklines and the formation of secondary bed forms. On the other hand, cellular automaton models have shown to be efficient to analyze pattern formation, and more particularly, the emergence of a hierarchy of bed forms [*Narteau et al.*, 2009]. Often described as reduced complexity models, these discrete numerical methods allow for fast computation of significant portions of dune fields over long times, especially because they are constructed from an elementary length scale that incorporates all the diversity of the smaller scale processes [*Rozier and Narteau*, 2014]. Furthermore, in most of the cellular automaton models, individual cells can be identified and tracked to quantitatively estimate their migration history. Here we exploit such a property in a 3-D model to study the motions of sediment particles in steady state barchans. Thus, we can estimate the residence time distribution of sediment particles in a barchan, i.e., the amount of time individual particles contribute to the overall dynamics of a barchan.

2. A Real-Space Cellular Automaton Dune Model

Cellular automata models are discrete systems that combine and iterate different sets of rules on a network of interacting cells [*Chopard and Droz*, 1998]. In a vast majority of cases, each of these cells are in a finite

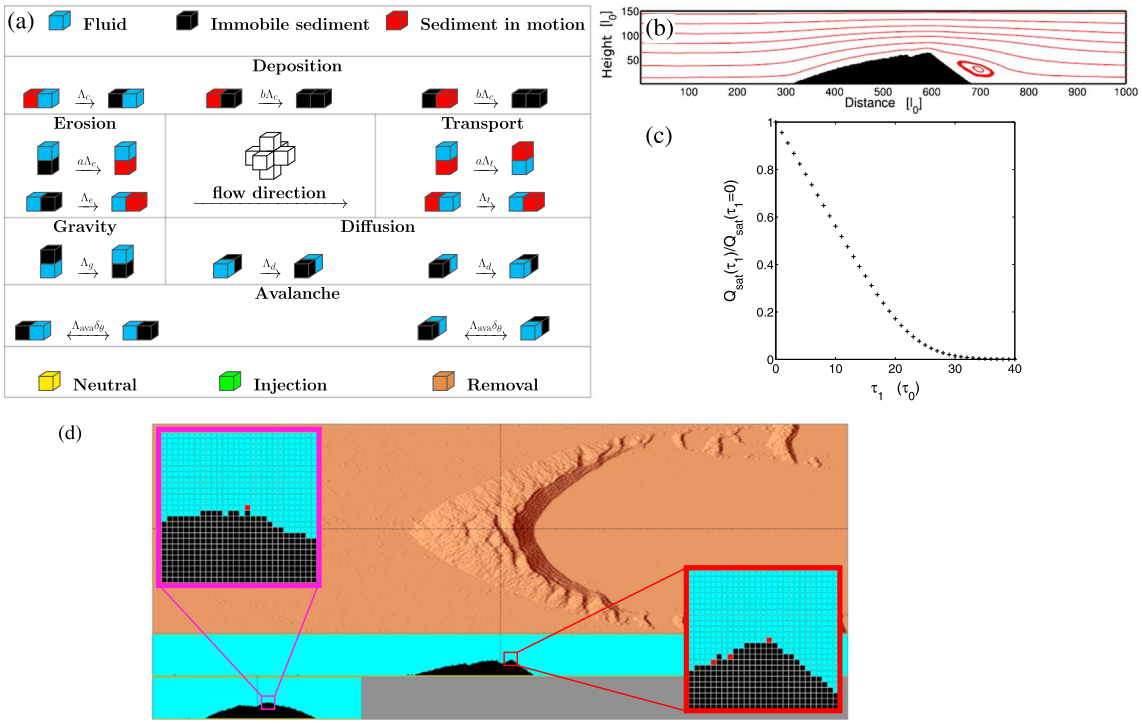

Figure 1. A 3-D real-space cellular automaton dune model. (a) Active transitions of doublets in the cellular automaton model for sediment transport. Different sets of transition are associated with deposition, erosion, transport, gravity, diffusion, and avalanche. Transition rates with units of frequency are Λ_c, Λ_e, Λ_t, Λ_g, Λ_d, and Λ_{ava}; a and b are constants. The central inset shows the direction of the flow and the orientation of the nearest neighbors in a regular cubic lattice. See equation (5) for the definition of δ_θ and Tables 1 and 2 for all the other parameter values. (b) Velocity streamlines above a barchan using the lattice-gas cellular automaton. (c) The saturated flux Q_{sat} measured on a flat sand bed with respect to the τ_1 value. Q^0_{sat}, the Q_{sat} value at $\tau_1 = 0$, is used as a normalization constant. (d) The topography of a barchan in the cellular automaton dune model. Dashed lines correspond to the longitudinal and the transverse vertical slices of cells shown below. Two insets zoom in on regions of high sediment transport to show individual cells that can be tracked at the surface of the dune but also within the dune during a turnover cycle.

number of states, and network connections are simplified to include only nearest neighbors interactions. Then cellular automaton are known to produce collective patterns and large-scale phenomena as a result of both negative and positive feedbacks.

The real space cellular automaton dune model combines a cellular automaton of sediment transport with a lattice-gas cellular automaton for high Reynolds-flow simulation [*Narteau et al.*, 2009; *Zhang et al.*, 2010, 2012]. In the model of sediment transport, we consider three states (fluid, mobile, and immobile sediment) and local interactions between pairs of nearest neighbor cells called doublets (Figure 1a). The elementary length scale of the cubic lattice is the characteristic length scale l_0 of the model. At this length scale, we isolate individual physical processes and associate each of them with a set of doublet transitions and a specific transition rate [*Narteau et al.*, 2001; *Narteau*, 2006]. This way, we introduce the characteristic time scales of the physical mechanisms under consideration (erosion, transport, deposition, gravity, and diffusion). These scales are expressed in units of t_0, the elementary time scale of the model. In addition, to reproduce all types of boundary conditions, neutral cells are used to shape the virtual environment and removal/injection states can locally control the intensity of output/input fluxes over time.

We use a lattice-gas model to simulate the flow and calculate the permanent feedback between bed shear stress and topography [*Frisch et al.*, 1986; *Chopard and Droz*, 1998; *Rothman and Zaleski*, 2004]. This flow is computed in 2-D vertical planes confined by two walls of neutral cells at the top and the bottom of the model of sediment transport. Thus, we neglect the effect of transverse secondary flows which are known to slightly contribute with opposite signs to tractional transport on the stoss and lee sides of dunes. More importantly, we impose no-slip boundary conditions on the bed surface and free-slip boundary conditions along the ceiling as a first approximation of a free surface. In the direction of the flow, we use periodic boundary conditions that ensure that the mean vertical component of the reinjected flow is null.

Table 1. Units of the Parameters of the Model of Sediment Transport

Elementary Units		Units
l_0	Length	$[L]$
t_0	Time	$[T]$
τ_0	Stress	$[M][L]^{-1}[T]^{-2}$

Using the output of the lattice-gas cellular automaton, we estimate both components of the local velocity field by averaging the velocity vectors of fluid particles over space and time. Velocity $\vec{V}$ is expressed in terms of a number of fluid particles and we use the normal $\vec{n}$ to the topography to calculate the bed shear stress (Figure 1b)

$$\tau_s = \tau_0 \frac{\partial \vec{V}}{\partial \vec{n}} \tag{3}$$

where τ_0 is the stress scale of the model (see Tables 1 and 2). Then we consider that the erosion rate is linearly related to the bed shear stress τ_s according to

$$\Lambda_e = \begin{cases} 0 & \text{for } \tau_s \le \tau_1 \\ \Lambda_0 \dfrac{\tau_s - \tau_1}{\tau_2 - \tau_1} & \text{for } \tau_1 \le \tau_s \le \tau_2 \\ \Lambda_0 & \text{else} \end{cases} \tag{4}$$

where Λ_0 is a constant rate, τ_1 is the threshold for motion inception, and τ_2 is a parameter to adjust the slope of the linear relationship. For consistency, we always have $\tau_s \ll \tau_2$. Most importantly, we can associate changes in τ_1 values to variations in excess shear stress and therefore to variations in shear velocity and flow strength: The higher the τ_1 value is, the lower the wind shear velocity is. Then for all τ_1 values, we can compute the saturated sand flux on a flat bed and renormalize this flux with respect to its maximum value at $\tau_1 = 0$ (Figure 1c).

In the model, we consider a so-called diffusion process to simulate transverse motions of sedimentary cells. In nature, this process results from lateral grain motions and involves a large number of physical processes, including grain-grain collisions and 3-D turbulent fluid flows [*Sauermann*, 2001; *Hersen*, 2004a; *Schwämmle and Herrmann*, 2005]. In the numerical simulations, the diffusion rate combines all these processes together in a single parameter Λ_d. As a consequence, this parameter may be related to the flow strength and any other parameter that influences transport. For the sake of simplicity, we do not account for such dependencies here; we prefer to consider Λ_d as a constant.

As in nature, avalanching in the model can also produce longitudinal and transverse motions of sedimentary cells. In addition to the diffusion process, it is the only other source of lateral sediment flux in the simulations. To minimize artifacts related to the cubic lattice, we introduce a new avalanche module based on a diffusion with threshold mechanism. The threshold is simply the repose angle θ_c of the granular material. In practice, we consider all the horizontal transitions between immobile sediment and fluid states (Figure 1). The corresponding transition rates are not constant over time and depend on the local slope θ as follows

$$\Lambda_\theta = \Lambda_{\text{ava}} \delta_\theta \quad \text{with} \quad \delta_\theta = \begin{cases} 0 & \text{if } \theta \le \theta_c \\ 1 & \text{if } \theta > \theta_c \end{cases} \tag{5}$$

In order to ensure that the slope is never larger than $\theta_c = 35°$, $\Lambda_{\text{ava}} \gg \Lambda_e$ in all the numerical simulations described below (see Tables 1 and 2).

An important property of our 3-D real-space cellular automaton dune model is that it tracks positions and motions of individual sedimentary cells (Figure 1d). Thus, even if we are not able to discuss the detailed exchange of grains below the elementary length scale l_0, we are able to follow the dynamics of the elementary particles to examine their migration history.

Table 2. Transition Rates and Values of the Parameters of the Model of Sediment Transport[a]

Model Parameters		Units	Value
L_s	System width and length	l_0	[300 and 1000]
H_s	System height	l_0	60
Λ_0	Transition rate for erosion	$1/t_0$	1
Λ_t	Transition rate for transport	$1/t_0$	1.5
Λ_c	Transition rate for deposition	$1/t_0$	0.5
Λ_g	Transition rate for gravity	$1/t_0$	10^5
Λ_d	Transition rate for diffusion	$1/t_0$	0.01
Λ_{ava}	Transition rate for avalanche	$1/t_0$	10
a	Erosion/transport coefficient	1	0.1
b	Deposition coefficient	1	10
$\tau_2 - \tau_1$	Erosion range	τ_0	100

[a]Transition rates for erosion, deposition, and transport are chosen close to one with $\Lambda_c < \Lambda_0 < \Lambda_t$. Gravity (Stokes' law) and diffusion are occurring over much shorter and longer periods of time, respectively. We chose $\Lambda_c \ll \Lambda_0 \ll \Lambda_t$. $a < 1$ corresponds to the ratio between vertical and horizontal transition rates for erosion and transport, $b > 1$ corresponds to the ratio between deposition rates on flat and rough surfaces (see Figure 1).

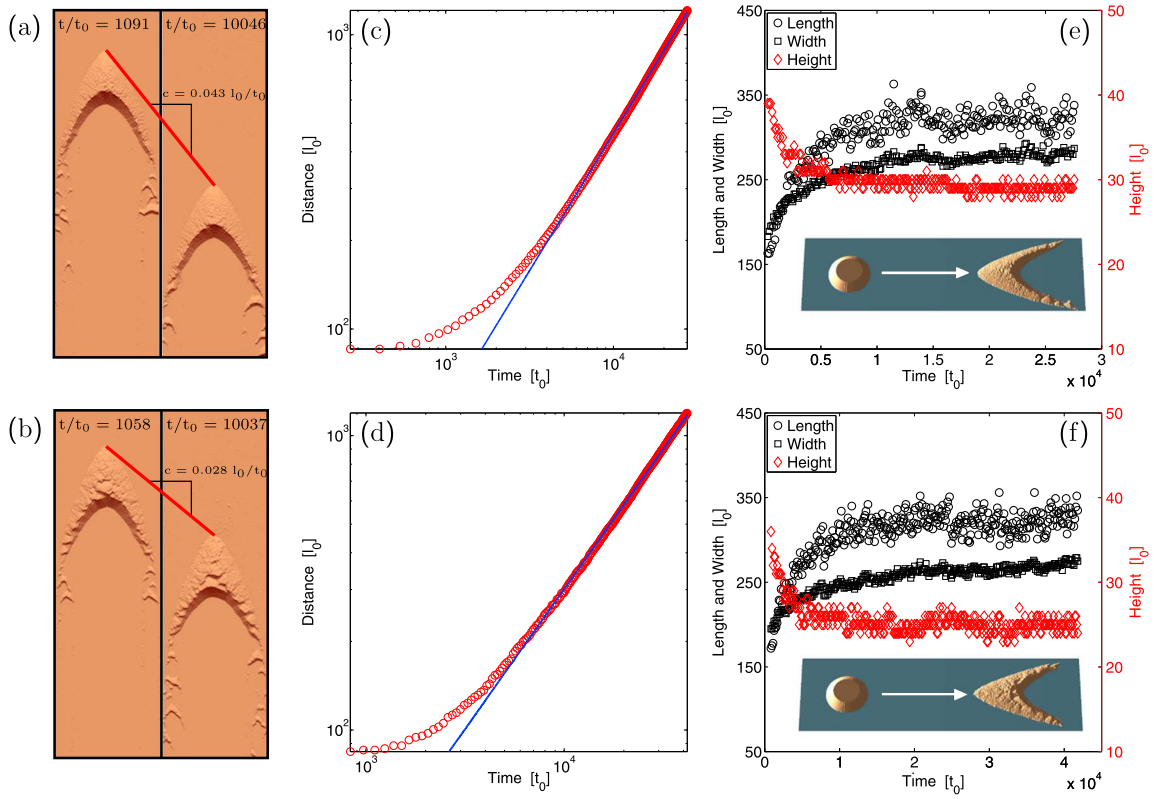

Figure 2. Barchans in quasi-stationary equilibrium states for high and low flows: (a) $\tau_1/\tau_0 = 1$ and (b) $\tau_1/\tau_0 = 20$. The initial condition at $t = 0$ is a truncated conical sand pile. All the sedimentary cells ejected downstream are randomly reinjected upstream. (c and d) Position of the center of mass and (e and f) evolution of the length, width, and height of the sand pile with respect to time. Over a short time, some sediment is redistributed within the entire system and the dune accelerates as it decreases in height. Over a long time, the steady state barchans are characterized by constant propagation speed and size. Note that superimposed bed forms are responsible for the systematic fluctuations of the dune dimensions.

3. Morphodynamics of a Steady State Barchan

First, we simulate steady state barchans with balanced inflow and outflow of sediment. The physical environment in the model consists of a flat bedrock and a ceiling which are laterally limited by two vertical walls of neutral cells facing each other at a distance D. The initial condition is a truncated conical sand pile placed upstream in the center of the system. Using the same numerical model, *Zhang et al.* [2010] have shown that barchans are not scale-invariant objects and that their shapes may evolve according to their size and the strength of the flow. Then we vary the volume of the initial sand pile and the flow strength (i.e., different τ_1 values, see equation (4)) to explore a wide range of dune shapes. The downstream border is made of removal cells to eliminate all sedimentary cells that reach this limit. At the upstream border, a line of injection cells is inserted in the ground in order to reinject uniformly all the sedimentary cells that have been removed at the opposite border.

For fast and slow flows, Figure 2 shows that barchans reach quasi-stationary equilibrium states with superimposed bed forms. As in nature, the dune instability is always responsible for the nucleation of secondary bed forms on the stoss side of larger dunes in the model [*Narteau et al.*, 2009]. Nevertheless, as these incipient dune features grow downstream, their amplitude depends on flow strength and on the slope of the sand bed on which they propagate [*Zhang et al.*, 2010]. Hence, the characteristic dimensions of the barchans need to be averaged over time to eliminate the shorter scale fluctuations associated with secondary bed forms (Figures 2e and 2f). Then each dune can be characterized by its propagation speed c (Figures 2c and 2d), length L_∞, width W_∞, height H_∞, volume V_∞, and output sedimentary flux Q_{out}, which is obviously equal to its input sedimentary flux Q_{in} when measured across the entire width of the system.

Following *Narteau et al.* [2009], Table 3 shows how these numerical simulations can be used to quantitatively predict the morphodynamics of (1) aeolian barchans in deserts on Earth, (2) subaqueous barchans on Earth, and (3) aeolian barchans on Mars. In practice, all the values in Table 3 are derived from the systematic

Table 3. Setting the Length and Time Scales $\{l_0, t_0\}$ of the Model to Quantify the Morphodynamics of Barchans in Different Geophysical Environments[a]

	Dunes in the Model	Terrestrial Aeolian Dunes ♁	Terrestrial Subaqueous Dunes ♒	Martian Aeolian Dunes ♂
λ_{max}[b]	40 l_0	20 m	$2 \cdot 10^{-2}$ m	600 m
Length scale $\Longrightarrow$	l_0	0.5 m	$5 \cdot 10^{-4}$ m	15 m
Motion threshold[c]	τ_1/τ_0	0.19 m/s	0.0062 m/s	0.69 m/s
		High flow strength τ_1/τ_0 =1 (Figure 2a)		
Barchan length L_∞	323 l_0	161.5 m	0.16 m	4845 m
Barchan width W_∞	279 l_0	139.5 m	0.14 m	4185 m
Barchan height H_∞	29 l_0	14.5 m	0.015 m	435 m
Q_{sat}/Q^0_{sat} (Figure 1c)	0.95	Ø	Ø	Ø
u_*[d]	Ø	0.85 m/s	0.03 m/s	3.09 m/s
Q_{sat}[e]	0.22 l_0^2/t_0	10^3 m^2/yr	883 m^2/yr	204 m^2/yr
Time scale[f] $\Longrightarrow$	t_0	$5.3 \cdot 10^{-5}$ year	$6.2 \cdot 10^{-11}$ year	0.24 year
Barchan velocity c	0.043 l_0/t_0	406 m/yr	345 km/yr	2.69 m/yr
		Low flow strength τ_1/τ_0 =20 (Figure 2b)		
Barchan length L_∞	322 l_0	161 m	0.16 m	4830 m
Barchan width W_∞	266 l_0	133 m	0.13 m	3990 m
Barchan height H_∞	25 l_0	12.5 m	0.013 m	375 m
Q_{sat}/Q^0_{sat} (Figure 1c)	0.17	Ø	Ø	Ø
u_*[d]	Ø	0.21 m/s	0.01 m/s	0.75 m/s
Q_{sat}[e]	0.04 l_0^2/t_0	12.5 m^2/yr	63.10 m^2/yr	1.94 m^2/yr
Time scale[f] $\Longrightarrow$	t_0	$8.0 \cdot 10^{-4}$ year	$1.58 \cdot 10^{-10}$ year	4.64 year
Barchan velocity c	0.028 l_0/t_0	17.5 m/yr	88.6 km/yr	0.09 m/yr

[a] λ_{max} is the characteristic length scale for the formation of dunes on a flat sand bed, u_* the shear velocity, u_{c*} the threshold shear velocity for sediment motion, d the grain diameter, ρ_g the grain density, ρ_f the density of the atmosphere, ρ_w the density of water and g the gravity. On Earth, we take d = 200 μm, ρ_{air} = 1.2 kg/m^3, $\rho_w = 10^3$ kg/m^3, $\rho_g = 2.5 \cdot 10^3$ kg/m^3, and g = 9.81 m/s^{-2}. On Mars, we take d = 87 μm, ρ_f = 0.02 kg/m^3, $\rho_g = 3 \cdot 10^3$ kg/m^3, and g = 3.7 m/s^2 [*Claudin and Andreotti*, 2006]. Although these laws may evolve from a physical environment to another, we systematically take the following:

[b] $\lambda_{max} = 50(\rho_s/\rho_f)d$ [*Elbelrhiti et al.*, 2005],

[c] $u_c = 0.1\sqrt{(\rho_s/\rho_f)gd}$ [*Bagnold*, 1936; *Iversen and Rasmussen*, 1999],

[d] $Q_{sat} = 25(\rho_f/\rho_s)\sqrt{d/g}(u_*^2 - u_c^2)$ [*Ungar and Haff*, 1987],

[e] $u_* = u_c \Big/ \sqrt{1 - Q_{sat}/Q^0_{sat}}$, and

[f] $t_0 = (Q_{sat}(\tau_1)/Q_{sat}(u_*))\, l_0^2$ [*Narteau et al.*, 2009]. In this last equation, $Q_{sat}(\tau_1)$ is the saturated flux in the model in units of $\{l_0, t_0\}$ and $Q_{sat}(u_*)$ is the saturated flux in nature in units of the international system.

comparison between the observed and the predicted behaviors, measured with the international system of units in nature and in units of $\{l_0, t_0\}$ in the model. For each geophysical environment, we first set the characteristic length scale l_0 of the model with respect to direct observations of λ_{max}, the characteristic length scale for the formation of dunes on a flat sand bed. Then we set the characteristic time scale t_0 by matching the average saturated flux in the model with relevant field observations [*Elbelrhiti et al.*, 2005]. In all cases, we use the same formulas to relate estimations of flow velocity to the shear velocity and ultimately the saturated flux (see caption of Table 3). This rescaling strategy relies on the assumption that the underlying physical processes are the same in the different geomorphic systems under investigation [*Claudin and Andreotti*, 2006]. Despite the fact that for each system specific processes may influence the overall development of bed forms, using the same theoretical framework provides insights into the relative size and speed of barchans in different environments. For example, with the same simulation in which $\tau_1/\tau_0 = 20$ (Figure 2b), we predict that 12 m high aeolian barchans on Earth propagate at a speed of 17 m/yr

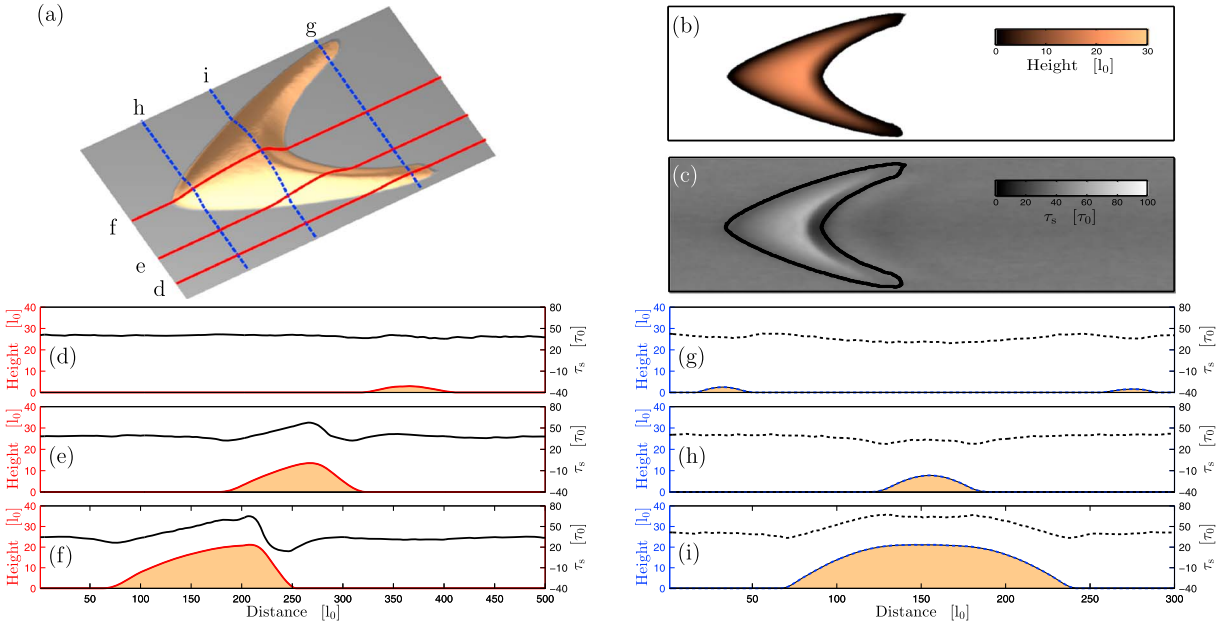

Figure 3. (a and b) Time-averaged topography and (c) basal shear stress of a barchan in a quasi-stationary equilibrium state (see Figure 2b, $\tau_1/\tau_0 = 20$). The temporal smoothing eliminates all perturbations induced by superimposed bed forms and allows the evaluation of dynamic equilibrium between flow and topography along (d–f) longitudinal and (g–i) transverse transects.

[*Hastenrath*, 1987; *Hesp and Hastings*, 1998], 13 mm high subaqueous barchans on Earth propagate at a speed of 10 m/h [*Hersen et al.*, 2002; *Groh et al.*, 2008], and 375 m high barchans on Mars propagate at a speed of 9 cm/yr [*Bridges et al.*, 2012].

In Figure 2b, the systematic occurrence of secondary bed forms illustrates that there are at least two levels of description for the barchans produced by the model. To leave the superimposed bed forms aside, we compute the mean dune shape and basal shear stress by temporal smoothing. In practice, the barchan at different times is shifted to the same position by minimizing the distance to four reference points: the upstream extremities of the windward and slip faces and the downstream extremities of the horns. Then we simply calculate the mean dune height and the mean basal shear stress at each point in space.

Figures 3a–3c show the smoothed topography and basal shear stress averaged from 100 configurations of the barchan uniformly sampled over a renewal time period (see equation (2)). These smoothed features are emergent properties that result only from patterns of interactions between the different cells over time [*Rozier and Narteau*, 2014]. Interestingly, they could be compared with similar features obtained with continuous models to benchmark numerical results against data. Most importantly for our present concern, the time-averaged properties can also be used to analyze lateral variations of the dynamic equilibrium between the topography and the flow (Figures 3d–3i).

Longitudinal slices show the disappearance of the slip face and a decreasing dune aspect ratio when moving from the center of the dune (Figure 3f) to the horns (Figure 3d). Not surprisingly, there is also an increase in shear stress up the stoss slope due to the compression and the acceleration of the flow (Figure 1c). Such a compression of streamlines is associated with a decreasing shear stress in the dune's toe region [*Wiggs*, 2001]. Above the slip face, the dune topography generates a flow separation, and the recirculation zone produces a sudden reduction in shear stress. Finally, streamlines reattach downstream and the basal shear stress recovers its stationary value for the flat sand bed upstream of the dune. Note that where the longitudinal dune profile exhibits a dome shape (Figure 3d) the absence of a slip face explains the gentle variations in basal shear stress. Perpendicular to the flow, transverse dune slices show an asymmetry in dune shape and basal shear stress between the stoss and lee sides of the dune (Figures 3g and 3h). In addition, the transverse slope of the stoss face increases as we move away from the center of the dune (Figure 3i).

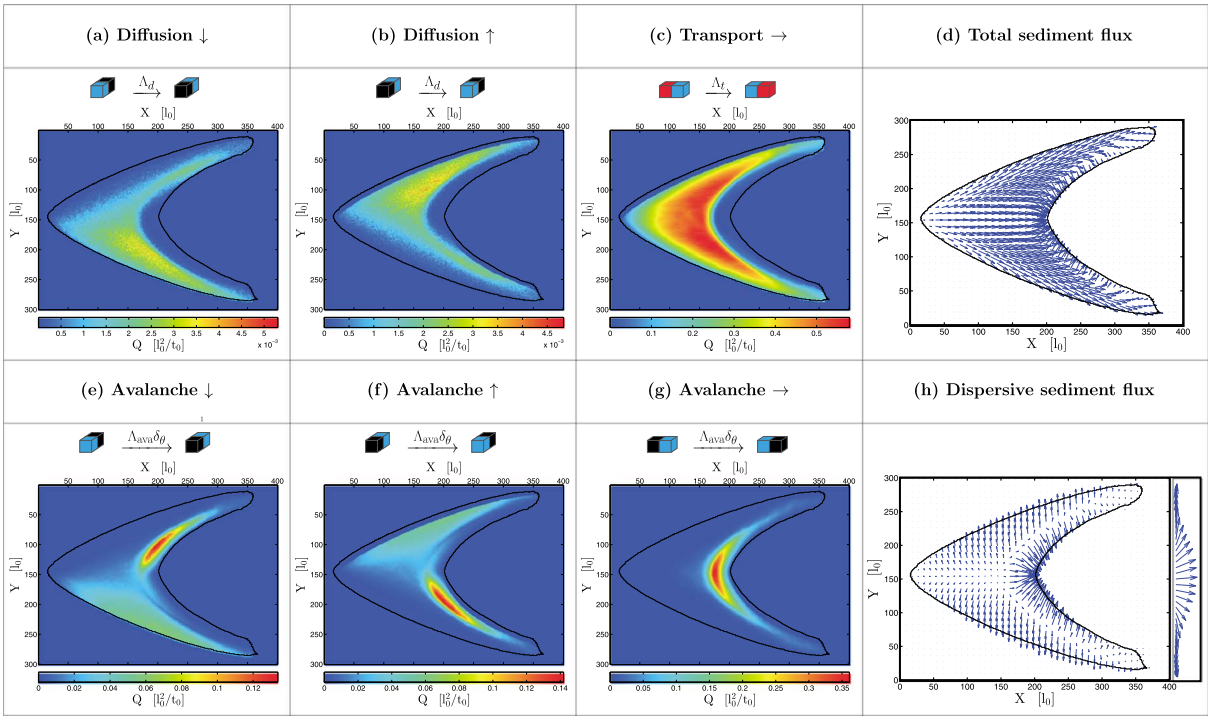

Figure 4. Decomposition of sediment fluxes on a barchan in a quasi-stationary equilibrium state: (a and b) diffusion, (c) bed load transport, and (e–g) avalanches. Orientation and intensity of the (d) total and (h) dispersive sediment fluxes on a barchan in a quasi-stationary equilibrium state (see Figure 2b, $\tau_1/\tau_0 = 20$). If all the transitions are taken into account for the total flux, only the transitions associated with diffusion (Figures 4a and 4b) and avalanching (Figures 4e–4g) contribute to the dispersive flux. Integrated longitudinally over the entire dune, the total dispersive flux on the barchan is shown as a vertical inset on the right of Figure 4h. Note that these fluxes may be directly related to the time-averaged topography and basal shear stress shown in Figure 3.

4. Residence Time and Migration History of Sediment Particles in Steady State Barchans

The time-averaged topography and basal shear stress of barchans can be locally related to the relative intensity of the physical mechanisms that contribute to the internal dynamics of the system. In practice, using our cellular automaton approach, we track individual sedimentary cells in space and time to associate their individual motions with specific transitions and the underlying physical mechanisms (Figure 1a).

4.1. Dispersive and Advective Sediment Fluxes on Barchans

Figure 4 shows the sediment fluxes associated with all the transitions that produce horizontal motions of sedimentary cells on a barchan. These fluxes can be divided into two categories. The first includes all the lateral dispersive processes, such as diffusion (Figures 4a and 4b) and avalanching (Figures 4e–4g). As expected from dune shape, these dispersive fluxes are symmetric with respect to the central longitudinal dune slice and change sign from stoss to lee slopes. The second category includes all the transport processes in the direction of the flow. In this case, we observe the predominance of bed load transport on the stoss slope (Figure 4c) and the predominance of avalanches on the lee slope (Figure 4g). By summing over all these fluxes, we can estimate the magnitude and the orientation of sediment transport over the entire dune.

Figure 4d shows the orientation of the overall sediment flux on a barchan. If the transport rate increases with height in response to an increasing shear stress (Figure 3c), the lateral dune slope is responsible for the transverse component of the sediment flux. Hence, Figure 4h shows the orientation and intensity of the sediment flux without the transition of transport (Figure 4c), considering only the transitions associated with diffusion (Figures 4a and 4b) and avalanches (Figures 4e–4g). Because an outward flux on the stoss slope is balanced by an inward flux on the lee slope, we also integrate them over each longitudinal dune slice to estimate the cumulative dispersive flux on a barchan (see the right vertical inset in Figures 4h). Not surprisingly, there is a net sediment transport from the center of the dune to the horns. This is a prerequisite to the stability of the barchan.

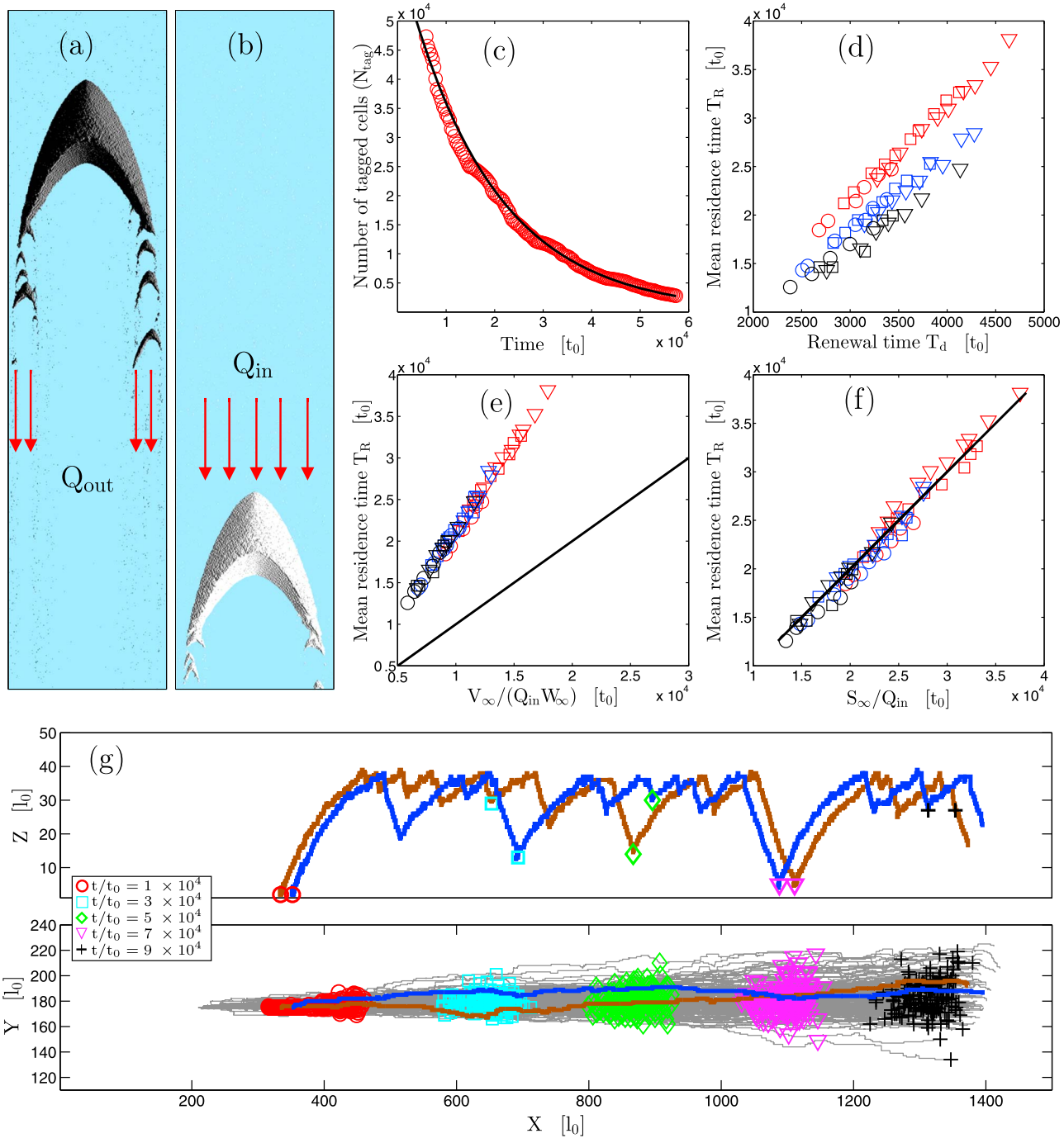

Figure 5. Mean residence time and motions of sedimentary cells in a barchan in a quasi-stationary equilibrium state. The steady state barchans at (a) $t = 0$ and (b) $t/t_0 = 5 \times 10^4$. The tagged and untagged sedimentary cells are shown in black and white, respectively. (c) Number of tagged sedimentary cells within the steady state barchan. The black curve is an exponential fit with a time constant $T_R/t_0 = 1.85 \times 10^4$ (see equation (6)). The mean residence time with respect to (d) the renewal time of the dune (see equation (2)) as well as with respect to (e) the volume of the dune, and (f) the surface of the longitudinal dune slice divided by their respective input sediment fluxes. In Figures 5e and 5f, the black $x = y$ lines represent an ideal solution for well-mixed reservoirs. Red, black, and blue symbols are for $\Lambda_d t_0$ values of 0.02, 0.06, and 0.1, respectively. Circles, squares, and triangles are for τ_1/τ_0 values of 1, 5, and 10, respectively. (g) Horizontal and vertical motions of sedimentary cells during the propagation of the steady state barchan. All tracked sedimentary cells originate from the central longitudinal dune slice. Two specific trajectories are shown in blue and brown. Symbols show the position of all the tracked particles at regular time intervals.

4.2. Residence Time and Motions of Particles in Steady State Barchans

Starting from a barchan in a quasi-stationary equilibrium state at $t = 0$ (Figure 5a), we track all sedimentary cells until they leave the system downstream. Thus, as the full simulation proceeds, we can follow individual particle motions, in particular when they are caught in avalanches or mobilized by the flow on both primary and superimposed bed forms. In practice, all sedimentary cells of the initial condition are tagged with an identification number, which is reset to 0 when the cells are randomly reinjected upstream. Thus, the proportion of tagged cells within the dune is continuously decreasing during its migration as the tagged cells ejected along horns are systematically replaced by the continuous input of untagged sedimentary cells (see the evolution from Figures 5a and 5b).

Using the same conditions as in Figure 2a, Figure 5c shows the number of tagged sedimentary cells that remain in the barchan with respect to time. This number decays exponentially

$$N_{tag}(t) \propto \exp\left(-\frac{t}{T_R}\right) \tag{6}$$

with a time constant T_R, which can be interpreted as a mean residence time of sedimentary cells within the barchan (i.e., the amount of time a particle contributes to the overall dynamics of the barchan). Such an exponential decay rate has been observed in all our numerical simulations. Then to estimate how the mean residence time depends on the dune morphology, we calculate the T_R value for a wide range of dune sizes ($5 \cdot 10^3 \leq V_\infty/l_0^3 \leq 10^4$), different diffusion rates ($\lambda_d t_0 \in \{0.02, 0.06, 0.1\}$), and various flow strengths ($\tau_1/\tau_0 \in \{1, 5, 10\}$). Figure 5d shows that the mean residence time is linearly related to the barchan renewal time T_d (see equation (2)). This dependency of residence time on dune speed may appear trivial, but it does not depend only on the factors that influence the dispersion of individual sedimentary cells in the dune during its propagation. In addition, the dune may be described as a reservoir that exchanges its material with its environment. Then, the residence time of a sediment particle in a barchan should be related to the ratio between the volume of the dune V_∞ and its total input sediment flux $Q_{in}W_\infty$. Figure 5e shows that it is the case, but the slope of the linear relationship is larger than one, indicating that there is not a systematic global mixing of sediment during the propagation of barchans. Finally, looking for the best relationship, we find that the mean time a particle spends in a barchan is directly equal to the surface of the central longitudinal dune slice divided by the input sediment flux (Figure 5f). Thus, the central longitudinal dune slice seems to impose its characteristic renewal time scale to the whole barchan.

In addition to the statistical properties of a large number of particles, tagged sedimentary cells can also be used to investigate the migration history of individual particles within the cellular space. Basically, we choose different particles and track their position through the system over time. For example, Figure 5g shows the trajectories of cells initially located at the base of central longitudinal dune slices during the propagation of the barchan. These particle pathlines are characterized by rapid propagation phases and long periods of stability as they are repeatedly re-exposed on the stoss face and reburied on the lee face. As a result of the dispersive processes (see Figure 4h), the sedimentary cells are redistributed throughout the entire dune as they slowly drift toward the horns. Nevertheless, this flux of particles cannot be modeled by a single diffusive process since it depends on the responses of a variety of physical processes to lateral changes in dune morphology. Independently, it is important to note that the depth at which a particle is buried during avalanches is a random variable. Then, the distribution of the time delay between two transport phases may be wider than usually expected.

5. Discussion

A barchan is an isolated bed form that propagates downstream when the flow re-activates of particles that have been buried in the lee. Thus, the entire surface of the barchan is either eroding or accreting and all grains move as the dune migrates over its length. There is no static granular layer where grains could replace each other, keeping the flux and the topography unchanged. Therefore, there is no need of a granular transport model to investigate the overall dynamics of individual grains and, as it is generally the case for dune morphodynamics, the results presented here do not depend strongly on the rebounding probability of impacting grains or the entrainment probability of surface grains.

A barchan is an open system that interacts with its environment through the emission of sediment along horns and the inflow of sediment on its stoss side. The mean sediment residence time is, on average, the total time a particle spends between first entering the barchan and finally leaving it. For large well-mixed reservoirs at equilibrium, it is commonly admitted that the residence time follows an exponential distribution with a characteristic time scale which is the ratio between the volume of the reservoir and the input flux [*Bolin and Rodhe*, 1973]. Here, we observe such exponential behavior for barchans in a quasi-stationary equilibrium state and we can conclude that the probability distribution function of the residence time of a sand grain in a barchan is

$$f(t) = \lambda_R \exp(-\lambda_R t) \tag{7}$$

with $\lambda_R = 1/T_R$ a characteristic frequency. Thus, the fraction of incoming grains in the barchan during the interval $(t, t + dt)$ is $f(t)dt$.

Most importantly, we show that the mean residence time T_R is not directly proportional to the volume of the dune or its renewal time (Figure 5e). In fact, we find that a particle remains in a barchan on a characteristic time scale which is much longer than the time it takes to recycle all the volume of the dune through input and output sediment fluxes. Instead, the T_R value is equal to the renewal time of the sediment in the central longitudinal dune slice. Thus, the slice with the slowest renewal process controls the sediment renewal rate of the entire dune. This indicates that a barchan is not a well-mixed sediment compartment. Rather, it should be subdivided into two reservoirs at least, a fast one and a slow one associated with the horns and the central part, respectively. Because of opposite dispersive fluxes on the windward and lee faces, particles from the central region may move from one side of the dune to the other and enter the same longitudinal slice several times during their journeys throughout the dunes. Then, as they move toward the horns, they are more and more likely to stay on the same side of the dune and considerably increase the probability of ejection.

Our results suggest that morphology of the central longitudinal slice contains most of the relevant information about the morphodynamics of a barchan in a quasi-stationary equilibrium state. However, such an ideal state never exists in natural environments where barchan are shaped by complex wind regimes and evolve over time according to variable input sand flux and/or collisions. At the length scale of a dune field of symmetric barchans (i.e., two arms of the same length), these fluctuating boundary conditions may be considered as noise, and the mean residence time of particles may be estimated from the largest longitudinal dune slice. In this case, the dune size distribution is enough to infer the total time a particle spends in the barchan dune field. On the other hand, if barchans show a systematic asymmetry, the migration history of sediment particles may change considerably as a result of oblique dune motions [i.e. *Ping et al.*, 2014]. This specific type of dune should be analyzed independently using appropriate simulations.

The mean residence time in barchans may be related to the time scale of the so-called transverse instability that transforms transverse dunes in a set of independent barchans [*Hersen*, 2004b]. Indeed, in both cases, the coupling of longitudinal dune slices by lateral transport determines, in turn, the height and the velocity of each slice. *Parteli et al.* [2011] have shown that a transverse dune is globally unstable because a difference in height accelerates the smallest longitudinal dune slice and is then amplified by lateral flows associated with avalanches. In our case, we show that when there is an input sand flux, the overall dispersive flux may be stronger on the windward face than on the lee face [*Niiya et al.*, 2012; *Guignier et al.*, 2013]. This may be an important stabilizing factor which was not taken into account by *Parteli et al.* [2011].

Classic dune models that implement a set of differential equations use, in the vast majority of cases, a height-integrated mass flux that prevents the identification of individual particle motions. Using a real-space cellular automaton approach, we have shown that tagged particles and particle tracking may yield precise estimates of migration history of sedimentary cells. Obviously, we do not work at the grain scale and all the results must be discussed with respect to the elementary length scale, l_0. However, with this caveat in mind, the particle tracking techniques presented in this paper may be a powerful numerical tool to analyze basic problems of sediment transport in different types of geophysical environments where the residence time distribution remains controversial. This is especially the case in dune fields with abundant sand supply where sediment particles may participate in the formation and the propagation of bed forms or be stored for much longer periods in zones of deposition. Taken into account the fact that we also know the depth at which each sedimentary cell is buried at any time, the numerical outputs of our 3-D real-space

cellular automaton may also be directly compared to other dating methods, such as optically-stimulated luminescence [*Yang et al.*, 2006; *Zhou et al.*, 2012] and cosmogenic nuclides in quartz [*Vermeesch et al.*, 2010]. There is no doubt that our understanding in the physics of sand dunes may benefit from these new observational constraints.

6. Conclusion

To understand how long a sand grain contributes to the morphodynamics of a barchan before it is ejected along the horns, we use a particle tracking technique to explore lateral transport and sediment dispersion in steady state barchans produced by a 3-D real-space cellular automaton dune model. We show that barchans cannot be considered as well-mixed reservoirs. Furthermore, the mean residence time of a single particle is equal to the surface of the central longitudinal dune slice divided by the inflow of sediment. From a more general perspective, we conclude that there is critical need for new types of numerical methods to comprehensively describe the sediment residence time in geomorphic systems. Ideally, these new simulations would provide the entire migration history of individual particles. Such information can then be translated into depths and times to derive specific properties (e.g., burial history, last exposure time, and transport rates) that can be independently measured using geochemical dating techniques or tracers.

Acknowledgments

We are grateful to Eric Gayer, Sylvain Courrech du Pont, and Sébastien Rodriguez for helpful discussions. The paper has been improved by constructive comments of David Rubin, Hiraku Nishimori, Pieter Vermeesch, and an anonymous reviewer. The research was supported by the National Natural Science Foundation of China (grants 40930105, 41172325, and 41302146) and the China Postdoctoral Science Foundation (grant 2013M541031). We also acknowledge financial support from the UnivEarthS LabEx program of Sorbonne Paris Cité (ANR-10-LABX-0023 and ANR-11-IDEX-0005-02) and the French National Research Agency (ANR-09-RISK-004/GESTRANS and ANR-12-BS05-001-03/EXO-DUNES).

References

Andreotti, B., P. Claudin, and S. Douady (2002), Selection of dune shapes and velocities part 1: Dynamics of sand, wind and barchans, *Eur. Phys. J. B*, *28*, 321–339.

Bagnold, R. A. (1936), The movement of desert sand, *Proc. R. Soc. London, Ser. A*, *157*, 594–620.

Bagnold, R. A. (1941), *The Physics of Blown Sand and Desert Dunes*, 265 pp., Methuen, London.

Birnbaum, G., et al. (2010), Strong-wind events and their influence on the formation of snow dunes: Observations from Kohnen station, Dronning Maud Land, Antarctica, *J. Glaciol.*, *56*, 891–902.

Bolin, B., and H. Rodhe (1973), A note on the concepts of age distribution and transit time in natural reservoirs, *Tellus*, *25*, 58–62.

Bourke, M. C. (2010), Barchan dune asymmetry: Observations from Mars and Earth, *Icarus*, *205*, 183–197.

Bridges, N., F. Ayoub, J. Avouac, S. Leprince, A. Lucas, and S. Mattson (2012), Earth-like sand fluxes on Mars, *Nature*, *485*, 339–342.

Brown, E. T., R. F. Stallard, M. C. Larsen, G. M. Raisbeck, and F. Yiou (1995), Denudation rates determined from the accumulation of in situ produced ^{10}Be in the Luquillo experimental forest, Puerto Rico, *Earth Planet. Sci. Lett.*, *129*, 193–202.

Chopard, B., and M. Droz (1998), *Cellular Automata Modeling of Physical Systems*, Cambridge Univ. Press, Cambridge.

Claudin, P., and B. Andreotti (2006), A scaling law for aeolian dunes on Mars, Venus, Earth, and for subaqueous ripples, *Earth Planet. Sci. Lett.*, *252*, 30–44.

Dosseto, A., B. Bourdon, and S. P. Turner (2008), Uranium-series isotopes in river materials: Insights into the timescales of erosion and sediment transport, *Earth Planet. Sci. Lett.*, *265*, 1–17, doi:10.1016/j.epsl.2007.10.023.

Edgett, K. S., and D. G. Blumberg (1994), Star and linear dunes on Mars, *Icarus*, *112*, 448–464.

Elbelrhiti, H., P. Claudin, and B. Andreotti (2005), Field evidence for surface-wave-induced instability of sand dunes, *Nature*, *437*, 720–723.

Finkel, H. J. (1959), The barchans of southern Peru, *J. Geol.*, *67*, 614–647.

Fischer, S., M. E. Cates, and K. Kroy (2008), Dynamic scaling of desert dunes, *Phys. Rev. E*, *77*, 031,302–031,307, doi:10.1103/PhysRevE.77.031302.

Franklin, E. M., and F. Charru (2011), Subaqueous barchan dunes in turbulent shear flow. Part 1. Dune motion, *J. Fluid Mech.*, *675*, 199–222.

Frisch, U., B. Hasslacher, and Y. Pomeau (1986), Lattice-gas automata for the navier-stokes equation, *Phys. Rev. Lett.*, *56*, 1505–1508.

Gao, X., D. Zhang, O. Rozier, and C. Narteau (2013), Transport capacity and saturation mechanism in a real-space cellular automaton dune model, *Adv. Geosci.*, *37*, in press.

Gayer, E., S. Mukhopadhyay, and B. J. Meade (2008), Spatial variability of erosion rates inferred from the frequency distribution of cosmogenic ^{3}He in olivines from Hawaiian river sediments, *Earth Planet. Sci. Lett.*, *266*, 303–315, doi:10.1016/j.epsl.2007.11.019.

Groh, C., A. Wierschem, N. Aksel, I. Rehberg, and C. Kruelle (2008), Barchan dunes in two dimensions: Experimental tests for minimal models, *Phys. Rev. E*, *78*, 021,304.

Guignier, L., H. Niiya, H. Nishimori, D. Lague, and A. Valance (2013), Sand dunes as migrating strings, *Phys. Rev. E*, *87*, 052,206.

Hastenrath, S. (1987), The barchan dunes of southern Peru revisited, *Z. Geomorphol.*, *31*, 167–178.

Hersen, P. (2004a), On the crescentic shape of barchan dunes, *Eur. Phys. J. B*, *37*, 507–514.

Hersen, P. (2004b), Morphogénèse et dynamique des barchans, PhD thesis, Université Paris 7.

Hersen, P. (2005), Flow effects on the morphology and dynamics of aeolian and subaqueous barchan dunes, *J. Geophys. Res.*, *110*, F04S07, doi:10.1029/2004JF000185.

Hersen, P., S. Douady, and B. Andreotti (2002), Relevant length scale of barchan dunes, *Phys. Rev. Lett.*, *89*, 264,301.

Hesp, P. A., and K. Hastings (1998), Width, height and slope relationships and aerodynamic maintenance of barchans, *Geomorphology*, *22*, 193–204.

Howard, A. D., J. B. Morton, M. Gad El Hak, and D. B. Pierce (1978), Sand transport model of barchan dune equilibrium, *Sedimentology*, *25*, 307–338.

Iversen, J. D., and K. Rasmussen (1999), The effect of wind speed and bed slope on sand transport, *Sedimentology*, *46*, 723–731.

Kroy, K., G. Sauermann, and H. J. Herrmann (2002), Minimal model for aeolian sand dunes, *Phys. Rev. E*, *66*, 031,302.

Lancaster, N. (2008), Desert dune dynamics and development: Insights from luminescence dating, *Boreas*, *37*, 559–573.

Momiji, H., and A. Warren (2000), Relations of sand trapping efficiency and migration speed of transverse dunes to wind velocity, *Earth Surf. Proc. Land.*, *25*, 1069–1084.

Momiji, H., H. Nishimori, and S. R. Bishop (2002), On the shape and migration speed of a proto-dune, *Earth Surf. Proc. Land.*, *27*, 1335–1338.

Narteau, C. (2006), Formation and evolution of a population of strike-slip faults in a multiscale cellular automaton model, *Geophys. J. Int.*, *168*, 723–744.
Narteau, C., J. L. Le Mouël, J. P. Poirier, E. Sepúlveda, and M. Shnirman (2001), On a small-scale roughness of the core–mantle boundary, *Earth Planet. Sci. Lett.*, *191*, 49–60.
Narteau, C., D. Zhang, O. Rozier, and P. Claudin (2009), Setting the length and time scales of a cellular automaton dune model from the analysis of superimposed bed forms, *J. Geophys. Res.*, *114*, F03006, doi:10.1029/2008JF001127.
Niiya, H., A. Awazu, and H. Nishimori (2012), Bifurcation analysis of the transition of dune shape under unidirectional wind, *Phys. Rev. Lett.*, *108*, 158,001, doi:10.1103/PhysRevLett.108.158001.
Nishimori, H., and N. Ouchi (1993), Computational models for sand ripple and sand dune formation, *Int. J. Mod. Phys. B*, *7*, 2025–2034.
Nishimori, H., M. Yamasaki, and K. H. Andersen (1998), A simple model for the various pattern dynamics of dunes, *Int. J. Mod. Phys. B*, *12*, 257–272.
Parteli, E. J. R., J. S. Andrade Jr., and H. J. Herrmann (2011), Transverse instability of dunes, *Phys. Rev. Lett.*, *107*, 188,001.
Ping, L., C. Narteau, Z. Dong, Z. Zhang, and S. Courrech du Pont (2014), Emergence of oblique dunes in a landscape-scale experiment, *Nat. Geosci.*, *7*, 99–103, doi:10.1038/ngeo02047.
Pye, K., and H. Tsoar (1990), *Aeolian Sand and Sand Dunes*, Unwin Hyman, London.
Rothman, D. H., and S. Zaleski (2004), *Lattice-Gas Cellular Automata: Simple Models of Vomplex Hydrodynamics*, Cambridge Univ. Press, Cambridge.
Rozier, O., and C. Narteau (2014), A real-space cellular automaton laboratory, *Earth Surf. Proc. Land.*, *39*, 98–109, doi:10.1002/esp.3479.
Sauermann, G. (2001), Modeling of wind blown sand and desert dunes, PhD thesis, Universitat Stuggart.
Sauermann, G., K. Kroy, and H. J. Herrmann (2001), Continuum saltation model for sand dunes, *Phys. Rev. E*, *64*, 031,305.
Sauermann, G., J. S. Andrade, L. Maia, U. M. S. Costa, A. D. Araújo, and H. J. Herrmann (2003), Wind velocity and sand transport on a barchan dune, *Geomorphology*, *54*, 245–255.
Schmidt, K.-H., and P. Ergenzinger (1992), Bedload entrainment, travel lengths, step lengths, rest periods-studied with passive (iron, magnetic) and active (radio) tracer techniques, *Earth Surf. Proc. Land.*, *17*(2), 147–165.
Schwämmle, V., and H. J. Herrmann (2005), A model of barchan dunes including lateral shear stress, *Eur. Phys. J. E*, *16*, 57–65.
Taniguchi, K., N. Endo, and H. Sekiguchi (2012), The effect of periodic changes in wind direction on the deformation and morphology of isolated sand dunes based on flume experiments and field data from the western Sahara, *Geomorphology*, *179*, 286–299.
Ungar, J. E., and P. K. Haff (1987), Steady state saltation in air, *Sedimentology*, *34*, 289–299.
Van Rijn, L. C. (1993), *Principles of Sediment Transport in Rivers, Estuaries and Coastal Seas*, vol. 1006, Aqua Publications, Amsterdam.
Vermeesch, P., C. R. Fenton, F. Kober, G. F. S. Wiggs, C. S. Bristow, and S. Xu (2010), One million year residence time of Namib dune sand from cosmogenic nuclides, *Nat. Geosci.*, *3*, 862–865.
Vigier, N., B. Bourdon, S. Turner, and C. J. Allègre (2001), Erosion timescales derived from U-decay series measurements in rivers, *Earth Planet. Sci. Lett.*, *193*, 549–563, doi:10.1016/S0012-821X(01)00510-6.
Wasson, R. J., and R. Hyde (1983), Factors determining desert dune type, *Nature*, *304*, 337–339.
Werner, B. T. (1995), Eolian dunes: Computer simulations and attractor interpretation, *Geology*, *23*, 1107–1110.
Werner, B. T., and D. T. Gillespie (1993), Fundamentally discrete stochastic model for wind ripple dynamics, *Phys. Rev. Lett.*, *71*, 3230–3233.
Wiggs, G. F. S. (2001), Desert dune processes and dynamics, *Prog. Phys. Geogr.*, *25*, 53–79.
Yang, X., F. Preusser, and U. Radtke (2006), Late quaternary environmental changes in the Taklamakan desert, western China, inferred from OSL-dated lacustrine and aeolian deposits, *Quaternary Sci. Rev.*, *25*, 923–932.
Yang, X., H. Li, and A. Conacher (2012), Large-scale controls on the development of sand seas in northern China, *Quatern. Int.*, *250*, 74–83.
Zhang, D., C. Narteau, and O. Rozier (2010), Morphodynamics of barchan and transverse dunes using a cellular automaton model, *J. Geophys. Res.*, *115*, F03041, doi:10.1029/2009JF001620.
Zhang, D., C. Narteau, O. Rozier, and S. C. du Pont (2012), Morphology and dynamics of star dunes from numerical modelling, *Nat. Geosci.*, *5*, 463–467.
Zhou, J., Y. Zhu, and C. Yuan (2012), Origin and lateral migration of linear dunes in the Qaidam basin of NW China revealed by dune sediments, internal structures, and optically stimulated luminescence ages, with implications for linear dunes on titan, *Geol. Soc. Am. Bull.*, *124*, 1147–1154.